



Observation of superconductivity and its enhancement at the charge density wave critical point in LaAgSb₂

Kazuto Akiba ^{*}, Nobuaki Umeshita, and Tatsuo C. Kobayashi

Graduate School of Natural Science and Technology, Okayama University, Okayama 700-8530, Japan

 (Received 25 July 2022; revised 22 September 2022; accepted 13 October 2022; published 27 October 2022)

We discover superconductivity (SC) in LaAgSb₂ at ambient pressure and its close correlation with a charge density wave (CDW) under pressure. The superconducting transition temperature (T_c) exhibits a sharp peak at a CDW critical pressure of 3.2 GPa. We demonstrate that the carriers inhabiting the Sb-square net are crucial not only in the formation of CDW but also in SC for their relatively strong electron-phonon coupling (EPC). Furthermore, theoretical EPC strength in pristine LaAgSb₂ cannot explain the observed peak with $T_c \sim 1$ K, which indicates that an additional mechanism reinforces SC only around the CDW critical pressure.

DOI: [10.1103/PhysRevB.106.L161113](https://doi.org/10.1103/PhysRevB.106.L161113)

A correlation between the superconductivity (SC) and other orders can help identify the mechanism behind SC and offers insight to improve the superconducting transition temperature (T_c). A well-known example is the correlation between SC and magnetism. When a magnetic phase transition temperature is continuously suppressed toward absolute-zero temperature by an external parameter, a phase transition can be triggered even at 0 K, which is known as a quantum critical point (QCP). Around the QCP, various physical quantities demonstrate anomalous temperature (T) dependence due to the spin fluctuation [1], which is called non-Fermi-liquid behavior. Interestingly, unconventional SCs have been observed near the pressure- (P -) induced QCP in several heavy fermion systems [2–4], which result in a dome-like superconducting phase in the T - P phase diagram. This suggests that the spin fluctuation plays an important role on the pairing mechanism in this material class.

Alternatively, the correlation between SC and the charge density wave (CDW) has also attracted considerable attention. In several representative materials, the emergence of SC or a substantial enhancement of T_c occurs near the CDW critical point [5–9], which is often associated with a nonmonotonic change of power law in the ρ - T curve at low temperatures [6,7]. Intriguingly, these phenomena have several similar features as those of the magnetic QCP case, which suggests that these two phenomena have a possible commonality. However, a lack of model materials has hindered the elucidation of the essential relationship between SC and CDW.

Herein, we focus on the layered intermetallic compound LaAgSb₂ as an ideal platform to achieve the aforementioned goals. At ambient pressure, LaAgSb₂ exhibits sequential CDW transitions at $T_{\text{CDW1}} = 210$ K and $T_{\text{CDW2}} = 190$ K [10,11], whose critical pressures are determined as $P_{\text{CDW1}} \sim 3.2$ GPa and $P_{\text{CDW2}} \sim 1.7$ GPa, respectively [12]. Although the origin of CDW2 is not conclusive at present, CDW1 is

assumed to be derived from the nesting within the characteristic hollow-shaped Fermi surface (FS) [11,13,14]. Previous studies have reported that the hollow-shaped FS exhibits a Dirac-like linear dispersion at the Fermi level [15,16]. The emergence of linear band crossing in Sb- or Bi-square-net materials can be understood as a result of band folding associated with the 4⁴-net structure [17–19]. Intriguingly, isostructural compounds LaAuSb₂ [20] and LaCuSb₂ [21] show superconductivity at 0.6 and 0.9 K, respectively, the former of which coexists with CDW order. However, a report on SC in LaAgSb₂ is lacking.

In this Letter, we report the discovery of bulk SC in LaAgSb₂ at ambient pressure with $T_c \sim 0.3$ K. SC exhibits intimate correlation with CDW1 under high pressure, and T_c is significantly enhanced up to $T_c \sim 1$ K only around P_{CDW1} . The theoretical calculation demonstrates that the Sb-square net is crucial not only as a host of Dirac fermions and CDW1, but also as a primary superconducting layer. In addition, theoretical T_c of pristine LaAgSb₂ cannot reproduce the peak structure under pressure, which suggests that an additional reinforcement mechanism of SC activated only around the CDW critical point exists.

Single crystals of LaAgSb₂ were synthesized using the Sb self-flux method [10,12]. Temperatures as low as 50 mK were realized using a homemade ³He/⁴He dilution refrigerator. High pressure was generated using an indenter-type pressure cell (IPC, $P < 4$ GPa) [22] and opposed-anvil-type pressure cell (OAPC, $P < 7$ GPa) [23]. Daphne oil 7474 [24] was used as a pressure medium. The pressure in the sample space was determined based on the T_c of Pb set near the sample. The resistivity measurements were performed using a model 370 ac resistance bridge (Lake Shore Cryotronics, Inc.) following a standard four-terminal method. Magnetization measurements were performed using a dc superconducting quantum interference device (Tristan Technologies, Inc.). In the magnetization measurement, we did not intentionally apply an external magnetic field. The measurements were done in a residual geomagnetic field. Specific heat was measured by the relaxation method. The details of the magnetization and specific

^{*}akb@okayama-u.ac.jp

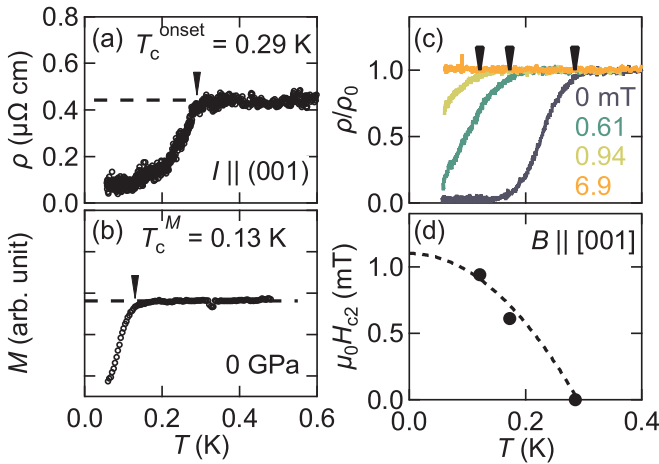


FIG. 1. (a) Temperature dependence of the in-plane resistivity ρ at ambient pressure. The onset temperature of the superconducting transition is determined as $T_c^{\text{onset}} = 0.29$ K. (b) Temperature dependence of the magnetization M at ambient pressure. The onset of the magnetization anomaly is determined as $T_c^M = 0.13$ K. (c) Temperature dependence of ρ normalized by the value at 0.4 K (ρ_0) under several external magnetic fields. Solid arrows indicate the onset of the superconducting transition. (d) Temperature dependence of the upper critical field $\mu_0 H_{c2}$ obtained from the data shown in (c). The dashed line represents $\mu_0 H_{c2}$ (mT) = $1.1[1 - (T/0.29)^2]$.

heat measurements are described in the Supplemental Material [25]. For resistivity and magnetization measurements, the sample was shaped into a rectangle with typical dimensions of $1 \times 0.5 \times 0.1$ mm³. For specific heat measurements, a relatively large as-grown crystal (typically several tens of milligrams) was used. First-principles calculations were performed by the QUANTUM ESPRESSO package [26–28] using scalar-relativistic ultrasoft pseudopotentials. Electron-phonon coupling (EPC) and T_c were calculated using the WANNIER90 [29] and EPW [30] codes. The visualization of orbital projections on FS was performed by FERMISURFER [31]. The calculation and verification of the results are described in detail in the Supplemental Material [25] (see also Refs. [32–36] therein).

Figure 1(a) shows the temperature dependence of the in-plane resistivity ρ [current within the (001) plane] at ambient pressure. The residual resistivity ratio deduced from ρ at 300 and 0.6 K was ~ 88 , and $T_{\text{CDW1}} = 210$ K was clearly observed (not shown). As depicted in Fig. 1(a), an abrupt decrease in ρ was observed, whose onset temperature can be defined as $T_c^{\text{onset}} = 0.29$ K, indicated by the arrow. This observation strongly suggests that the superconducting state exists at ambient pressure.

Figure 1(b) plots the temperature dependence of the magnetization M for an identical sample, which shows a distinct anomaly at $T_c^M = 0.13$ K. In addition, the superconducting volume fraction was estimated as $\sim 39\%$ at 60 mK, as described in the Supplemental Material [25]. Since the present measurement corresponds to field cooling under a residual geomagnetic field, the estimated volume fraction can be regarded as the lower limit. The incomplete shielding and apparent difference between T_c^M and T_c^{onset} are presumably

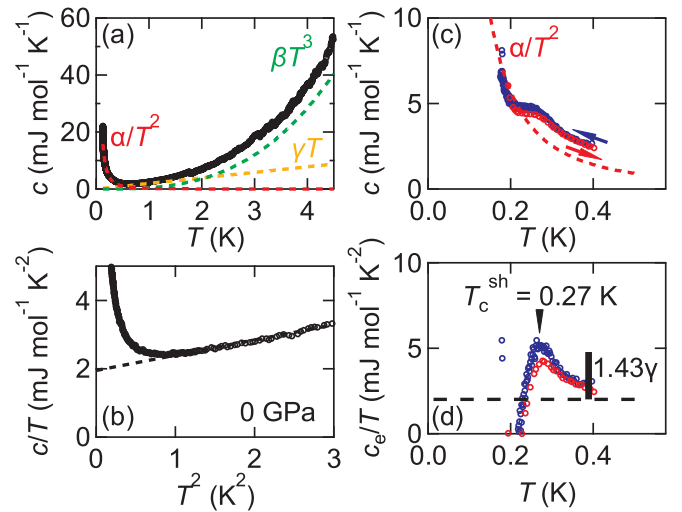


FIG. 2. (a) Temperature dependence of the specific heat c at ambient pressure. Dotted curves represent the individual contributions from nuclei (red), phonons (green), and electrons (orange). (b) c/T as a function of T^2 . The straight line represents the linear fit used for deducing the electron and phonon specific heat coefficients. (c) Specific heat anomaly below 0.5 K. Red and blue markers represent the heating and cooling processes, respectively. The dashed curve represents the nuclear contribution which is proportional to $1/T^2$. (d) c_e/T as a function of T , where c_e represents the electronic specific heat. The vertical scale represents the expected jump in BCS theory (~ 2.8 mJ mol⁻¹ K⁻²).

due to imperfect zero resistivity even at the lowest T and broad superconducting transition in this sample.

Figure 1(c) shows the temperature dependence of ρ normalized by the value at 0.4 K (ρ_0) under external magnetic fields along the [001] (crystallographic c) axis. We note that there is a sample dependence in the sharpness of the superconducting transition; in a sample investigated in Fig. 1(c), we can recognize more clear zero resistivity than Fig. 1(a). The onset temperature of the superconducting transition systematically decreases as the magnetic field increases, and SC is completely absent under 6.9 mT. We can estimate from Fig. 1(d) the upper critical field ($\mu_0 H_{c2}$) at 0 K as ~ 1.1 mT.

To obtain thermodynamic evidence, the specific heat at ambient pressure was measured. Figure 2(a) shows the temperature dependence of the specific heat c . Here, c is represented as $c = \alpha/T^2 + \beta T^3 + \gamma T$, where the first, second, and third term represent the nuclear, phonon, and electron contributions, respectively. At a relatively high temperature above 1 K, the nuclear contribution is negligibly small; thus, c is dominated by electron and phonon contributions. This results in the linear dependence in the c/T - T^2 plot, as shown in Fig. 2(b). From the slope and vertical intercept of the straight line, $\beta = (444 \pm 7)$ $\mu\text{J mol}^{-1} \text{K}^{-4}$ and $\gamma = (1.95 \pm 0.01)$ mJ mol⁻¹ K⁻² were obtained. From β , the Debye temperature was estimated as $\Theta_D = (48R\pi^4/5\beta)^{1/3} = 260$ K, where R represents the gas constant. The obtained γ and Θ_D are comparable to values reported in previous experiments [21,37]. In contrast, at temperatures below 1 K, a drastic increase in nuclear contribution was observed, as shown in Fig. 2(a), which is well scaled by α/T^2 with

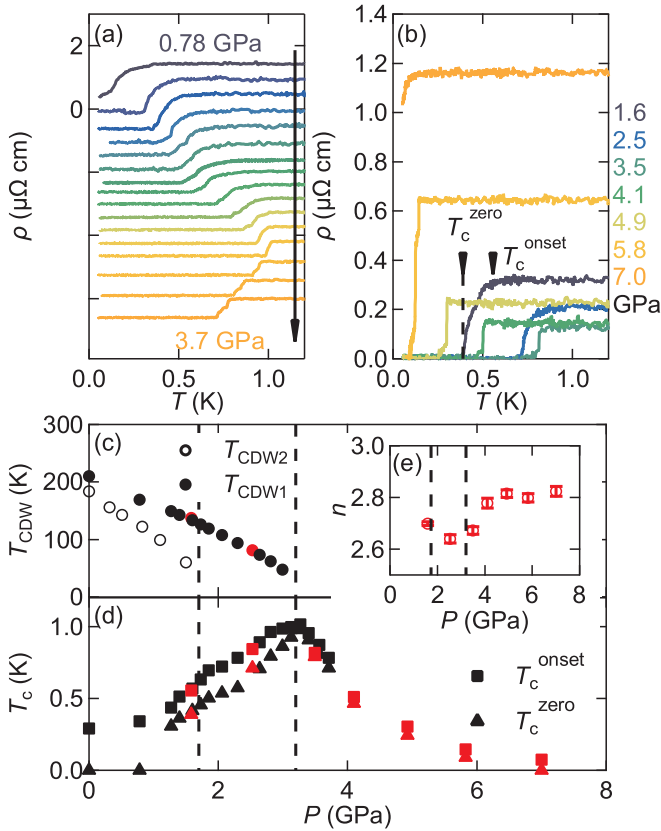


FIG. 3. Temperature dependence of ρ (a) up to 3.7 GPa measured using the indenter-type pressure cell (IPC) and (b) up to 7.0 GPa measured using the opposed-anvil-type pressure cell (OAPC). Each trace in (a) is vertically shifted for clarity. The definitions of T_c^{onset} and T_c^{zero} are indicated by arrows in the case of 1.6 GPa in (b). Pressure dependence of (c) CDW transition and (d) superconducting transition temperatures. The black and red markers represent the data obtained using IPC and OAPC, respectively. (e) Pressure dependence of power n in $\rho = \rho_0 + A'T^n$ over the range $2.5 \text{ K} < T < 35 \text{ K}$.

$\alpha = (259.4 \pm 0.5) \mu\text{J mol}^{-1} \text{ K}$. By first-principles calculation, we confirmed a notably large nuclear quadrupole resonance frequency of Sb due to the large electromagnetic field gradient around the Sb site, which is ascribed to be the origin of Schottky-type behavior below 1 K. Although the anomaly due to the superconducting transition is quite smaller than nuclear specific heat, a humplike anomaly can be discerned at $T_c^{\text{sh}} = 0.27 \text{ K}$, as shown in Fig. 2(c). Figure 2(d) shows c_e/T as a function of T , where the electronic specific heat c_e is obtained by subtracting the dashed curve in Fig. 2(c) from c . The magnitude of the anomaly shows reasonable agreement with $1.43\gamma \sim 2.8 \text{ mJ mol}^{-1} \text{ K}^{-2}$ [black vertical scale in Fig. 2(d)], which is expected from Bardeen-Cooper-Schrieffer (BCS) theory. This serves as firm evidence for bulk SC at ambient pressure.

From the above results, the coexistence of the CDWs and SC in LaAgSb₂ at ambient pressure was established. Subsequently, their correlation under pressure was investigated.

Figures 3(a) and 3(b) show the temperature dependence of ρ up to 3.7 GPa and up to 7.0 GPa, obtained using IPC and OAPC, respectively. The pressure dependence of CDW

and superconducting transition temperatures are summarized in Figs. 3(c) and 3(d), respectively. The consistency of the data obtained by IPC and OAPC is satisfactory. Herein, T_{CDW1} was determined from the data presented in the Supplemental Material [25], and T_{CDW2} was taken from our previous study [12]. The definitions of T_c^{onset} and T_c^{zero} are indicated in Fig. 3(b) by arrows. Although the transition was broad at pressures below 1 GPa, zero resistivity above 1.3 GPa was distinctly observed. Both T_c^{onset} and T_c^{zero} gradually increased with pressure and reached their maxima almost exactly at $P_{\text{CDW1}} = 3.2 \text{ GPa}$. A maximum onset temperature of $T_c^{\text{onset}} = 0.98 \text{ K}$ was found to be 3.4 times higher than that measured at ambient pressure. On the other hand, we can find no discernible anomaly at $P_{\text{CDW2}} \sim 1.7 \text{ GPa}$. Above P_{CDW1} , T_c immediately got suppressed, and its decrement rate was steeper than the increment below P_{CDW1} . This resulted in a distinct peak structure in the T - P phase diagram, as shown in Fig. 3(d). At the highest pressure of 7.0 GPa, $T_c^{\text{onset}} = 75 \text{ mK}$ was 1/13 compared to its maximum value, and T_c^{zero} was again below the lowest limit of the present study. The obvious correlation with CDW1 further confirms the bulk SC.

Here, we discuss the correlation between CDW1 and SC. Because LaAgSb₂ is a nonmagnetic material, the pairing mechanism is primarily assumed to be the EPC. Thus, we focused on the EPC strength in the momentum space at ambient pressure. In the following calculations, lattice modulation by CDWs was not considered, i.e., the results in pristine crystal structures without CDWs.

Figures 4(a) and 4(b) represent the distribution of the EPC strength λ_k on the $k_z = 0$ and $k_z = \pi/c$ planes, respectively. Carriers with a relatively strong EPC ($\lambda_k \sim 0.3$) are concentrated on the two-dimensional hollowlike surface and elongated pocket at the X point, whereas the rest of the FS exhibited weaker EPC ($\lambda_k = 0.1\text{--}0.15$). As shown in the Supplemental Material [25], this situation also holds under pressure. Because the hollowlike FS is the host of the CDW1 nesting, the above-mentioned results lead to the interpretation that the CDW1 and SC compete on identical FS, which results in their remarkable correlation.

Figures 4(c) and 4(d) show the orbital characters of the FS on the k_z planes described in Figs. 4(a) and 4(b). Notably the FSs with strong EPC are dominated by the intense $5p_{x,y}$ character of Sb1, which is a constituent of the Sb-square net. The population of other orbitals is relatively minor, as presented in the Supplemental Material [25]. These results indicate that the Sb-square net is responsible not only for the emergence of linear band crossing and nesting of CDW1 but also serves as a primary superconducting layer in this material. As we previously mentioned, no discernible anomaly of T_c at $P_{\text{CDW2}} \sim 1.7 \text{ GPa}$ was observed. Given that the SC is primarily responsible for the Sb- $p_{x,y}$, this behavior can be reasonably understood. The lattice modulation accompanied by CDW2 is known to be along the c axis [11], which is perpendicular to the orbital spread; thus, a rather minor effect on SC is expected. In contrast, CDW1 causes lattice modulation along the a axis [11] within the Sb-square net, which can directly affect the superconducting properties.

Here, we extend our quantitative discussion on the superconducting properties based on the McMillan-Allen-Dynes formalism [38–40]. Within this framework, the

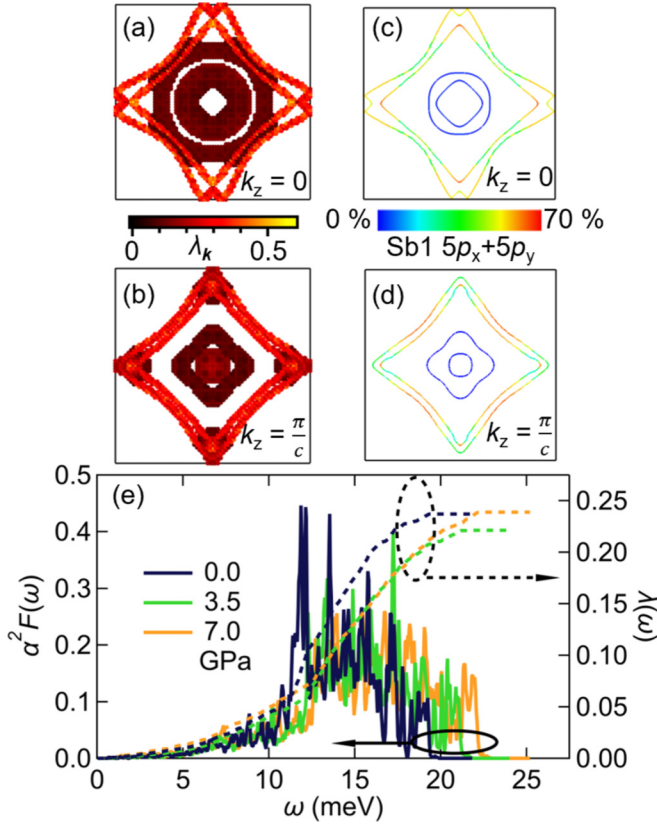


FIG. 4. Momentum-resolved electron-phonon coupling strength $\lambda_{\mathbf{k}}$ on (a) $k_z = 0$ and (b) $k_z = \pi/c$ planes at ambient pressure. $\lambda_{\mathbf{k}}$ is calculated for k points within the range of ± 0.2 eV from the Fermi level. The projection of $5p_x + 5p_y$ orbital character for Sb1 on (c) $k_z = 0$ and (d) $k_z = \pi/c$ planes at ambient pressure. (e) Eliashberg spectral function $\alpha^2F(\omega)$ (left axis) and integrated electron-phonon coupling strength $\lambda(\omega)$ (right axis) at 0, 3.5, and 7.0 GPa.

superconducting transition temperature T_c^{MAD} is represented as

$$T_c^{\text{MAD}} = \frac{\omega_{\log}}{1.2} \exp\left(-\frac{1.04(1 + \lambda)}{\lambda - \mu_c^*(1 + 0.62\lambda)}\right), \quad (1)$$

where $\lambda = \lambda(\omega_{\max})$ is the integrated EPC strength defined by

$$\lambda(\omega) = 2 \int_0^\omega d\omega' \frac{\alpha^2F(\omega')}{\omega'}, \quad (2)$$

and ω_{\log} is the logarithmic average of the phonon frequency defined as

$$\omega_{\log} = \exp\left(\frac{2}{\lambda} \int_0^{\omega_{\max}} d\omega \ln \omega \frac{\alpha^2F(\omega)}{\omega}\right), \quad (3)$$

where ω_{\max} denotes the maximum of the phonon frequency. $\alpha^2F(\omega)$ is the Eliashberg spectral function, which can be obtained from first-principles results, as described in the Supplemental Material [25]. The calculated $\alpha^2F(\omega)$ at 0, 3.5, and 7.0 GPa are presented in Fig. 4(e) with corresponding $\lambda(\omega)$ values; the resulting λ , ω_{\log} , and T_c^{MAD} are listed in Table I. To calculate T_c^{MAD} , we assumed a typical Coulomb pseudopotential of $\mu_c^* = 0.1$ for metals [41]. The obtained λ did not exhibit any notable pressure dependence. Accordingly,

TABLE I. Theoretical EPC strength (λ), experimental EPC strength (λ^{expt}), logarithmic average of phonon frequency (ω_{\log} , converted into temperature), and superconducting transition temperature estimated by the McMillan-Allen-Dynes formula (T_c^{MAD}) with the Coulomb pseudopotential $\mu_c^* = 0.1$.

P (GPa)	λ	λ^{expt}	ω_{\log} (K)	T_c^{MAD} (mK)
0.0	0.237	0.34	137.4	3.1
3.5	0.221	0.40	149.0	0.92
7.0	0.239	0.29	147.0	3.8

T_c^{MAD} was in the order of 1 mK at all pressures, which is three orders of magnitude smaller than the experimental maximum $T_c \sim 1$ K. Furthermore, the theoretical upper limit of T_c could be calculated by setting $\mu_c^* = 0$, i.e., by completely disregarding the Coulomb interaction. The averaged upper limit was ~ 0.49 K, which is lower than the experimental maximum.

Here, we can deduce the experimental EPC strength λ^{expt} based on [38]

$$\lambda^{\text{expt}} = \frac{1.04 + \mu_c^* \ln(\Theta_D/1.45T_c)}{(1 - 0.62\mu_c^*) \ln(\Theta_D/1.45T_c) - 1.04}. \quad (4)$$

Assuming $\Theta_D = 260$ K (estimated at ambient pressure), $\mu_c^* = 0.1$, and experimental T_c^{onset} , calculated λ^{expt} values are listed in Table I. At 7.0 GPa, far from P_{CDW1} , the difference between theoretical and experimental λ is small compared with other pressures, which supports the weak coupling nature of pristine LaAgSb₂. In contrast, near the P_{CDW1} , a λ nearly two times larger than the theoretical value is necessary to realize the observed maximum T_c assuming the EPC mechanism.

Consequently, the above results lead to a conclusion that there exists an additional mechanism that significantly reinforces the SC only around P_{CDW1} . In the real case, the CDW and superconducting gaps should compete for the density of states on the FS below P_{CDW1} [42]. Although this conventional picture may partially account for the increasing trend of T_c below P_{CDW1} , it cannot explain the significant difference in T_c between experiment and theory at P_{CDW1} and a rapid decrease above P_{CDW1} .

Since the above calculation does not explicitly consider the structural modification in the CDW states, we do not rule out an EPC origin, possibly related with a phonon softening by CDW1 formation [13,43], at the present stage. Another possible mechanism is of electronic origin, i.e., a charge fluctuation around P_{CDW1} . Assuming a spin-singlet SC, the effective interaction of the Cooper pairs $V^s(\mathbf{k}, \mathbf{k}')$ is given by $V^s(\mathbf{k}, \mathbf{k}') = U + 3U^2\chi_s(\mathbf{k} - \mathbf{k}')/2 - U^2\chi_c(\mathbf{k} - \mathbf{k}')/2$ [44], where U , $\chi_s(\mathbf{k} - \mathbf{k}')$, and $\chi_c(\mathbf{k} - \mathbf{k}')$ represent Coulomb repulsion, spin susceptibility, and charge susceptibility, respectively. Since the increase of χ_c brings a negative contribution on V^s , it can enhance the pairing attraction of the spin-singlet SC. Due to the coexistence of CDW1 and SC on identical FS and the absence of magnetism, the effect of charge fluctuation may stand out in the present case. We also note that a nonmonotonic change in the exponent n in $\rho = \rho_0 + AT^n$ was observed around 4 GPa, as shown in Fig. 3(e), which has been discussed in a context of possible quantum criticality at a CDW critical point [6,7]. To distinguish the

above possibilities, further rigorous considerations on EPC and the role of charge fluctuation on SC around P_{CDW1} must be addressed, which is beyond the scope of the present Letter. The detailed mechanism of the reinforcement of SC is left as an open question for future study.

In conclusion, we observed the coexisting SC and CDW states in LaAgSb₂ at ambient pressure and their close correlation under high pressure. The EPC calculations revealed that the Sb-square net plays a vital role not only in the formation of linear band crossing and CDW1 but also in the emergence

of SC. Our results highlight the strong reinforcement of SC activated only around the CDW1 critical point. LaAgSb₂ under high pressure serves as an ideal platform to elucidate the essence of the correlation between SC and CDW and to seek a route to improve T_c based on critical points of charge orders.

We thank J. Otsuki and H. Harima for valuable discussion and comments. This research was supported by JSPS KAKENHI Grants No. JP19K14660, No. JP21H01042, and No. JP22K14006.

-
- [1] T. Moriya, *Spin Fluctuation in Itinerant Electron Magnetism* (Springer, Berlin, 1985).
- [2] R. Movshovich, T. Graf, D. Mandrus, J. D. Thompson, J. L. Smith, and Z. Fisk, *Phys. Rev. B* **53**, 8241 (1996).
- [3] F. Grosche, S. Julian, N. Mathur, and G. Lonzarich, *Phys. B: Condens. Matter* **223**, 50 (1996).
- [4] N. D. Mathur, F. M. Grosche, S. R. Julian, I. R. Walker, D. M. Freye, R. K. W. Haselwimmer, and G. G. Lonzarich, *Nature (London)* **394**, 39 (1998).
- [5] E. Morosan, H. W. Zandbergen, B. S. Dennis, J. W. G. Bos, Y. Onose, T. Klimczuk, A. P. Ramirez, N. P. Ong, and R. J. Cava, *Nat. Phys.* **2**, 544 (2006).
- [6] A. F. Kusmartseva, B. Sipos, H. Berger, L. Forró, and E. Tutiš, *Phys. Rev. Lett.* **103**, 236401 (2009).
- [7] T. Gruner, D. Jang, Z. Huesges, R. Cardoso-Gil, G. H. Fecher, M. M. Koza, O. Stockert, A. P. Mackenzie, M. Brando, and C. Geibel, *Nat. Phys.* **13**, 967 (2017).
- [8] K. Y. Chen, N. N. Wang, Q. W. Yin, Y. H. Gu, K. Jiang, Z. J. Tu, C. S. Gong, Y. Uwatoko, J. P. Sun, H. C. Lei, J. P. Hu, and J.-G. Cheng, *Phys. Rev. Lett.* **126**, 247001 (2021).
- [9] F. H. Yu, D. H. Ma, W. Z. Zhuo, S. Q. Liu, X. K. Wen, B. Lei, J. J. Ying, and X. H. Chen, *Nat. Commun.* **12**, 3645 (2021).
- [10] K. D. Myers, S. L. Bud'ko, I. R. Fisher, Z. Islam, H. Kleinke, A. H. Lacerda, and P. C. Canfield, *J. Magn. Magn. Mater.* **205**, 27 (1999).
- [11] C. Song, J. Park, J. Koo, K.-B. Lee, J. Y. Rhee, S. L. Bud'ko, P. C. Canfield, B. N. Harmon, and A. I. Goldman, *Phys. Rev. B* **68**, 035113 (2003).
- [12] K. Akiba, H. Nishimori, N. Umeshita, and T. C. Kobayashi, *Phys. Rev. B* **103**, 085134 (2021).
- [13] A. Bosak, S.-M. Souliou, C. Faugeras, R. Heid, M. R. Molas, R.-Y. Chen, N.-L. Wang, M. Potemski, and M. Le Tacon, *Phys. Rev. Res.* **3**, 033020 (2021).
- [14] K. Akiba, N. Umeshita, and T. C. Kobayashi, *Phys. Rev. B* **105**, 035108 (2022).
- [15] K. Wang and C. Petrovic, *Phys. Rev. B* **86**, 155213 (2012).
- [16] X. Shi, P. Richard, K. Wang, M. Liu, C. E. Matt, N. Xu, R. S. Dhaka, Z. Ristic, T. Qian, Y.-F. Yang, C. Petrovic, M. Shi, and H. Ding, *Phys. Rev. B* **93**, 081105(R) (2016).
- [17] R. Hoffmann, *Angew. Chem. Int. Ed. Engl.* **26**, 846 (1987).
- [18] S. Klemenz, S. Lei, and L. M. Schoop, *Annu. Rev. Mater. Res.* **49**, 185 (2019).
- [19] S. Klemenz, A. K. Hay, S. M. L. Teicher, A. Topp, J. Cano, and L. M. Schoop, *J. Am. Chem. Soc.* **142**, 6350 (2020).
- [20] F. Du, H. Su, S. S. Luo, B. Shen, Z. Y. Nie, L. C. Yin, Y. Chen, R. Li, M. Smidman, and H. Q. Yuan, *Phys. Rev. B* **102**, 144510 (2020).
- [21] Y. Muro, N. Takeda, and M. Ishikawa, *J. Alloy. Compd.* **257**, 23 (1997).
- [22] T. C. Kobayashi, H. Hidaka, H. Kotegawa, K. Fujiwara, and M. I. Eremets, *Rev. Sci. Instrum.* **78**, 023909 (2007).
- [23] K. Kitagawa, H. Gotou, T. Yagi, A. Yamada, T. Matsumoto, Y. Uwatoko, and M. Takigawa, *J. Phys. Soc. Jpn.* **79**, 024001 (2010).
- [24] K. Murata, K. Yokogawa, H. Yoshino, S. Klotz, P. Munsch, A. Irizawa, M. Nishiyama, K. Iizuka, T. Nanba, T. Okada, Y. Shiraga, and S. Aoyama, *Rev. Sci. Instrum.* **79**, 085101 (2008).
- [25] See Supplemental Material at <http://link.aps.org/supplemental/10.1103/PhysRevB.106.L161113> for details of magnetization measurements, specific heat measurements, and theoretical calculations.
- [26] P. Giannozzi, S. Baroni, N. Bonini, M. Calandra, R. Car, C. Cavazzoni, D. Ceresoli, G. L. Chiarotti, M. Cococcioni, I. Dabo, A. D. Corso, S. de Gironcoli, S. Fabris, G. Fratesi, R. Gebauer, U. Gerstmann, C. Gougoussis, A. Kokalj, M. Lazzeri, L. Martin-Samos *et al.*, *J. Phys.: Condens. Matter* **21**, 395502 (2009).
- [27] P. Giannozzi, O. Andreussi, T. Brumme, O. Bunau, M. Buongiorno Nardelli, M. Calandra, R. Car, C. Cavazzoni, D. Ceresoli, M. Cococcioni, N. Colonna, I. Carnimeo, A. Dal Corso, S. De Gironcoli, P. Delugas, R. Distasio, A. Ferretti, A. Floris, G. Fratesi, G. Fugallo *et al.*, *J. Phys.: Condens. Matter* **29**, 465901 (2017).
- [28] M. Kawamura, Y. Gohda, and S. Tsuneyuki, *Phys. Rev. B* **89**, 094515 (2014).
- [29] G. Pizzi, V. Vitale, R. Arita, S. Bluegel, F. Freimuth, G. Géranton, M. Gibertini, D. Gresch, C. Johnson, T. Koretsune, J. Ibanez, H. Lee, J.-M. Lihm, D. Marchand, A. Marrazzo, Y. Mokrousov, J. I. Mustafa, Y. Nohara, Y. Nomura, L. Paulatto *et al.*, *J. Phys.: Condens. Matter* **32**, 165902 (2020).
- [30] S. Poncé, E. Margine, C. Verdi, and F. Giustino, *Comput. Phys. Commun.* **209**, 116 (2016).
- [31] M. Kawamura, *Comput. Phys. Commun.* **239**, 197 (2019).
- [32] S. L. Bud'ko, T. A. Wiener, R. A. Ribeiro, P. C. Canfield, Y. Lee, T. Vogt, and A. H. Lacerda, *Phys. Rev. B* **73**, 184111 (2006).
- [33] R. Singha, S. Samanta, T. S. Bhattacharya, S. Chatterjee, S. Roy, L. Wang, A. Singha, and P. Mandal, *Phys. Rev. B* **102**, 205103 (2020).
- [34] P. Ruzsala, M. Winiarski, and M. Samsel-Czekala, *Acta Phys. Pol. A* **138**, 748 (2020).
- [35] T. Takeuchi, A. Thamizhavel, T. Okubo, M. Yamada, N. Nakamura, T. Yamamoto, Y. Inada, K. Sugiyama, A. Galatanu, E. Yamamoto, K. Kindo, T. Ebihara, and Y. Ōnuki, *Phys. Rev. B* **67**, 064403 (2003).

- [36] F. Giustino, M. L. Cohen, and S. G. Louie, *Phys. Rev. B* **76**, 165108 (2007).
- [37] Y. Inada, A. Thamizhavel, H. Yamagami, T. Takeuchi, Y. Sawai, S. Ikeda, H. Shishido, T. Okubo, M. Yamada, K. Sugiyama, N. Nakamura, T. Yamamoto, K. Kindo, T. Ebihara, A. Galatanu, E. Yamamoto, R. Settai, and Y. Onuki, *Philos. Mag. B* **82**, 1867 (2002).
- [38] W. L. McMillan, *Phys. Rev.* **167**, 331 (1968).
- [39] R. C. Dynes, *Solid State Commun.* **10**, 615 (1972).
- [40] P. B. Allen and R. C. Dynes, *Phys. Rev. B* **12**, 905 (1975).
- [41] P. Morel and P. W. Anderson, *Phys. Rev.* **125**, 1263 (1962).
- [42] G. Bilbro and W. L. McMillan, *Phys. Rev. B* **14**, 1887 (1976).
- [43] R. Y. Chen, S. J. Zhang, M. Y. Zhang, T. Dong, and N. L. Wang, *Phys. Rev. Lett.* **118**, 107402 (2017).
- [44] Y. Yanase, T. Jujo, T. Nomura, H. Ikeda, T. Hotta, and K. Yamada, *Phys. Rep.* **387**, 1 (2003).